Characterization of Single-Tryptophan Mutants of Histidine-Containing Phosphocarrier Protein: Evidence for Local Rearrangements during Folding from High Concentrations of Denaturant†

Ana I. Azuaga,‡,§ Denis Canet,‡,||,⊥ Gerard Smeenk,# Roel Berends,# Fritz Titgemeijer,△ Ria Duurkens,# Pedro L. Mateo,▽ Ruud M. Scheek,# George T. Robillard,# Christopher M. Dobson,||,○ and Nico A. J. van Nuland*,§

Bijvoet Center for Biomolecular Research, University of Utrecht, Padualaan 8, 3584 CH, Utrecht, The Netherlands, Oxford Center for Molecular Sciences, University of Oxford, South Parks Road, Oxford OX1 3QT, U.K., GBB, University of Groningen, Nijenborgh 4, 9747 AG, Groningen, The Netherlands, Lehrstuhl für Mikrobiolgie, Friedrich-Alexander Universität Erlangen-Nürnberg, Strandtstrasse 5, 91058 Erlangen, Germany, and Facultad de Ciencias, Universidad de Granada, Av. Fuentenueva SN, 18071 Granada, Spain

Received November 15, 2002; Revised Manuscript Received January 28, 2003

ABSTRACT: We have used site-directed mutagenesis in combination with a battery of biophysical techniques to probe the stability and folding behavior of a small globular protein, the histidine-containing phosphocarrier protein (HPr). Specifically, the four phenylalanine residues (2, 22, 29, and 48) of the wild-type protein were individually replaced by single tryptophans, thus introducing site-specific probes for monitoring the behavior of the protein. The folding of the tryptophan mutants was investigated by NMR, DSC, CD, intrinsic fluorescence, fluorescence anisotropy, and fluorescence quenching. The heat-induced denaturation of all four mutants, and the GdnHCl-induced unfolding curves of F2W, F29W, and F48W, can be fitted adequately to a two-state model, in agreement with the observations for the wild-type protein. The GdnHCl unfolding transitions of F22W, however, showed the accumulation of an intermediate state at low concentrations of denaturant. Kinetic refolding studies of F2W, F29W, and F48W showed a major single phase, independent of the probe used (CD, fluorescence, and fluorescence anisotropy) and similar to that of the wild-type protein. In contrast, F22W showed two phases in the fluorescence experiments corresponding to the two phases previously observed in ANS binding studies of the wild-type protein [Van Nuland et al. (1998) *Biochemistry 37,* 622−637]. Residue 22 was found from NMR studies to be part of the binding interface on HPr for ANS. These observations indicate that the second slow phase reflects a local, rather than a global, rearrangement from a well-structured highly nativelike intermediate state to the fully folded native state that has less hydrophobic surface exposed to the solvent. The detection of the second slow phase by the use of selective labeling of different regions of the protein with fluorophores illustrates the need for an integrated approach in order to understand the intricate details of the folding reactions of even the simplest proteins.

Protein folding is the key step associated with the acquisition of biological activity by a polypeptide that has been synthesized on the ribosome. Protein folding is also involved in a wide range of biological processes from translocation across cell membranes and molecular trafficking to the control and regulation of cell growth and differentiation (*1*). Investigation of the fundamental mechanism of the folding process has primarily involved investigation of the refolding of proteins in vitro following denaturation, commonly by urea or guanidine hydrochloride (GdnHCl)[1] (*2*). The folding of most proteins has been found to involve the existence of one or more intermediate states during the transition from the fully unfolded to the fully native state. Nevertheless, the folding of small single-domain proteins, typically containing less than about 100 residues, has generally been observed to follow apparent two-state kinetics and to be fast (on the order of milliseconds), indicating that

† A.I.A. acknowledges financial support from the European Community TMR Program (FMBI960633), and P.L.M. acknowledges financial support from Spanish Grant BIO2000-1459. This work has been supported by the TMR Network, Structure and dynamics of intermediate states in protein folding, of the European Community (FMRX960013). The Oxford Center for Molecular Sciences is supported by EPSRC, BBSRC, and MRC. The research of C.M.D. is supported in part by a program grant from the Wellcome Trust.

* Corresponding author. Tel: +31-(0)30-2533295. Fax: +31-(0)30-2539254. E-mail: nuland@nmr.chem.uu.nl.

‡ These two authors contributed equally to this work.

§ University of Utrecht.

|| University of Oxford.

⊥ Present address: GeneProt Inc., 2 Pre-de-la-Fontaine, 1217 Meyrin/GE, Switzerland.

University of Groningen.

△ Friedrich-Alexander Universität Erlangen-Nürnberg.

▽ Universidad de Granada.

○ Present address: Department of Chemistry, University of Cambridge, Lensfield Road, Cambridge CB2 1EW, U.K.

[1] Abbreviations: AcP, acylphosphatase; ANS, 8-anilino-1-naphthalenesulfonic acid; CD, circular dichroism; DSC, differential scanning calorimetry; GdnHCl, guanidine hydrochloride; HPr, histidine-containing phosphocarrier protein; NMR, nuclear magnetic resonance; NOESY, nuclear Overhauser effect spectroscopy; TOCSY, total correlation spectroscopy.

10.1021/bi027182p CCC: $25.00
Published on Web 04/04/2003

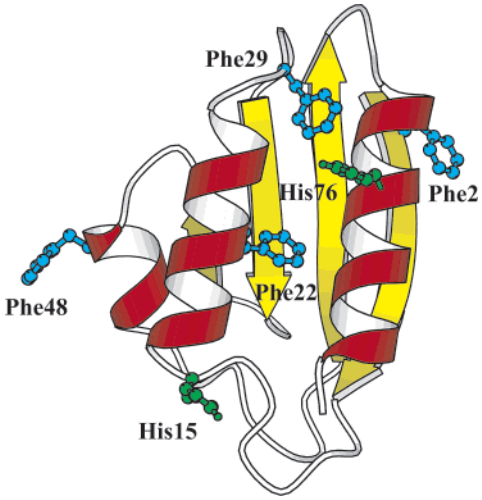

FIGURE 1: Molscript representation (*43*) of WT HPr. The four phenylalanine residues that were mutated and the two histidine residues are indicated in a ball-and-stick representation.

partially folded states are not significantly populated during the folding process (reviewed in ref *3*). This fact enables investigation of the most fundamental events in folding through characterization of transition state regions of the folding landscape (*3*−*6*). One class of protein that has been extensively studied to probe such aspects of folding is the acylphosphatase (AcP) family of proteins (*5*). Five members (AcP, ADA2h, U1A, MerP, and HPr) of this family of proteins have been investigated in total. They share a $\beta\alpha\beta\beta\alpha\beta$ fold, although they possess very low sequence homology. Despite their common fold, they span folding rates that vary by more than a factor of 3000. This observation can, however, be explained by differences in their relative contact order (*7*), a structural parameter that represents the normalized average separation in sequence between interacting residues (*8*). These proteins are therefore excellent systems through which to investigate common determinants of the acquisition of a specific topology (*7*).

One of the members of the AcP family of proteins is the histidine-containing phosphocarrier protein (HPr), a protein that plays a key role in the transport of carbohydrates across the cell membranes of bacteria via the phosphoenolpyruvate-dependent sugar phosphotransferase system (PTS). HPr catalyzes the transfer of a phosphoryl group from enzyme I to enzyme II, the membrane-bound transporter (*9*). The protein derived from *Escherichia coli* consists of 85 amino acid residues including two histidines; one of these, His15, forms part of the active site of the protein and the other, His76, is positioned in the C-terminal helix. The protein also contains four phenylalanines at positions 2, 22, 29, and 48. The structure of the protein has been determined by both NMR spectroscopy (*10*) and X-ray diffraction (*11*). It consists of three α-helices packed against a four-stranded antiparallel β-sheet in a $\beta\alpha\beta\beta\alpha\beta\alpha$ topology (Figure 1). On the basis of the structural similarity and the position of functionally important positively charged residues at the N-terminus of the first helix in HPr, AcP, and the RNA binding domain of ribonucleoproteins A and C, it was suggested that the observed fold of HPr represents a stable phosphate binding motif (*12*).

The small size and lack of disulfide bonds or cofactors in HPr make it an attractive system with which to study protein folding. Also, HPr folds slowly for a small protein (on the order of seconds), reflecting its relatively high contact order and making it accessible to study by a wide variety of biophysical techniques. As a consequence of the lack of tryptophan and tyrosine residues, however, the spectroscopic probes available for monitoring the folding of wild-type (WT) HPr are limited. Nevertheless, circular dichroism (CD) in the far- and near-ultraviolet (UV) and fluorescence associated with the binding of 8-anilino-1-naphthalenesulfonic acid (ANS) have been combined with nuclear magnetic resonance (NMR) spectroscopy and differential scanning calorimetry (DSC) to investigate equilibrium and kinetic features of the folding and unfolding process (*13*). From both types of studies it was found that the unfolding of HPr can be adequately described as a two-state process that does not involve significant accumulation of any intermediates. Refolding from high denaturant concentrations was found well described as a single-exponential process when monitored by stopped-flow far-UV CD and real-time NMR (*13*).

When folding of HPr was monitored by ANS binding, however, we detected deviations from this simple two-state behavior. Specifically, we observed the following: (i) double-exponential refolding kinetics, the main phase coinciding with the single phase observed using far-UV CD and NMR, (ii) a fluorescence overshoot in the dead time of the kinetic unfolding experiments, and (iii) an increase in fluorescence at low GdnHCl concentration during the equilibrium denaturation prior to the major cooperative transition. To understand the underlying origins of these features of the folding reaction, we have used an integrated approach, involving site-directed mutagenesis and the exploitation of a battery of complementary biophysical techniques, to probe the folding of HPr at specific sites in the structure. In this paper we describe a strategy by which the four phenylalanine residues in HPr were replaced by single tryptophans, thus introducing intrinsic probes that enable characterization of the stability and folding by fluorescence techniques. A particularly important finding is that, despite the near two-state behavior of the protein, a slow reorganization process is required during the folding prior to generation of the fully functional native state.

MATERIALS AND METHODS

Overproduction and Purification. DNA fragments containing the *ptsH* gene with a codon for a tryptophan instead of a phenylalanine were constructed using a two-step PCR procedure as described by Landt et al. (*14*). As a template the plasmid pRB1 containing the *ptsH* gene was used. PWO DNA polymerase was used to create blunt-ended products. The first PCR generated intermediate fragments that were purified over a column and used as "mega" primers in the second PCR together with the M13 reverse primer. The fragments were purified on agarose gel and ligated into the blunt-ended vector pBluescriptSK$^-$ cut with *Sma*I. DNA sequencing confirmed the replacement of the phenylalanine codon by a tryptophan codon in each of the four constructs. The expression plasmids were designated pRB2 (F2W), pRB4 (F48W), pRB6 (F22W), and pRB8 (F29W).

The production and purification of the mutant proteins were carried out as described for WT HPr (*15*). All

characterization and folding experiments were carried out using HPr buffered in solutions of 100 mM sodium phosphate (NaP_i) at pH 7.0. The phosphoryl-transfer function of the mutants was determined using a complementation assay that monitors the K_m value of the phosphotransferase reaction from HPr to enzyme IIA^{Mtl} (*16*). These measurements are done under saturating phosphorylated enzyme I concentrations so that all of the HPr is phosphorylated and that the concentration dependence of the rate of sugar phosphorylation is a measure of the quality of both the binding to enzyme IIA^{Mtl} and the rate of phosphorylation of enzyme IIA^{Mtl}. The K_m value of the WT protein was determined as a control. The molar extinction coefficients of the four single-tryptophan mutants of HPr were calculated from their amino acid composition (*17*). The concentrations of guanidine hydrochloride (GdnHCl) were checked by refractive index measurements as described by Pace (*18*).

Steady-State and Time-Resolved Fluorescence Spectroscopy. Steady-state fluorescence spectroscopy was carried out with a luminescence spectrometer, LS50B (Perkin-Elmer), using a quartz cuvette with a path length of 1 cm. The excitation wavelength was 280 nm with a band-pass of 5 nm, and the emission spectra were recorded from 300 to 400 nm with a band-pass of 7 nm. The concentration of the mutant HPr proteins was ca. 3 μM for F2W, F22W, and F48W and 13 μM for F29W in 100 mM NaP_i, pH 7.0. The time-resolved fluorescence spectroscopy experiments were performed at the Agricultural University of Wageningen as described by Visser et al. (*19*).

Nuclear Magnetic Resonance (NMR) Spectroscopy. NMR spectra were recorded either on home-built NMR spectrometers operating at 600.2 and 750.1 MHz in Oxford or on a 600 MHz Varian Inova in Groningen and processed using FELIX (Hare Research). Spectral widths were 8000 Hz at 600 MHz and 10000 Hz at 750 MHz. 2D NOESY spectra in H_2O and D_2O and a 2D TOCSY spectrum in H_2O of the WT HPr and the 2D NOESY spectra in D_2O of the mutant HPr proteins F2W, F22W, and F29W were recorded at 600 MHz. 2D NOESY spectra and 2D TOCSY spectra in H_2O of F2W, F22W, and F29W were recorded at 750 MHz. All experiments were run at 20 °C. The protein concentrations of the WT protein and the mutant proteins were ca. 1.2 and 2 mM, respectively. ^1H chemical shifts are expressed relative to sodium 2,2-dimethyl-2-silapentane-5-sulfonate (DSS).

Typical experimental details are as follows. NOESY spectra were recorded in H_2O at 750 MHz. The resolution in the first domain was 4K points, and 64 scans were accumulated. A total of 900 t_1 increments were recorded. The relaxation delay was 1 s, and the mixing time was 100 ms. The ^1H carrier frequency was at the water resonance. The latter was suppressed using a gradient double echo (*20*). The processing of the data was carried out using a 90° skewed sine-bell window function in the first domain and a Kaiser window function in the second domain. TOCSY spectra were recorded in H_2O at 750 MHz. Isotopic mixing was achieved using DIPSI-2 during 50.6 ms and suppression of cross-relaxation (NOE/ROE) using a delay of 0.5 times the mixing time. Further details were as described for the NOESY spectra recorded in H_2O. NOESY spectra were also recorded in D_2O at 600 MHz. The resolution in the first domain was 2K points, and 64 scans were accumulated. A total of 800 t_1 increments were recorded. The relaxation delay was 1 s, and the mixing time was 100 ms. The ^1H carrier frequency was at the water resonance. The latter was suppressed by weak on-resonance irradiation during the 1 s relaxation delay. The processing of the data was carried out using a 90° skewed sine-bell window function in the first domain and a Kaiser window function in the second domain. The 2D TOCSY and NOESY spectra were used for the assignment of the tryptophan resonances and identification of secondary structure elements.

Differential Scanning Calorimetry (DSC). Calorimetric experiments were carried out using a DASM 4 instrument with capillary cells of 0.47 mL, under a constant pressure of 2.5 atm and at a heating rate of 2 K/min (*21*) in Granada. Before the cell was filled, the samples were extensively dialyzed against the appropriate buffer solution. Reversibility of protein denaturation was assessed by comparison of the thermograms obtained in two consecutive scans with the same sample. After subtraction of the instrumental baseline from the original DSC recording in each case, the resulting endotherm was corrected for the effect of the calorimeter response as described previously (*22*). The temperature dependencies of the molar partial heat capacity, C_p, of the proteins were calculated from the DSC data as shown by Privalov and Potekhin using a partial specific volume of 0.73 mL/g (*23*). The thermal unfolding of all the mutant proteins occurred under equilibrium conditions; the C_p curves were fitted using a two-state model as described previously (*24*). All folding data described in this paper were fitted using the software package Origin (OriginLab, Northampton, MA) unless stated otherwise.

Equilibrium Denaturation by Circular Dichroism (CD). All CD studies were performed on a Jasco 720 spectrometer in Oxford using a quartz cuvette with a path length of 1 mm for the far-UV CD measurements. The GdnHCl transition curve at 20 °C was obtained using the Job method as described previously (*13*), initially recording far-UV CD spectra of samples of 20 μM protein solutions in 100 mM NaP_i, pH 7.0, containing 0 and 4.0 M GdnHCl. These samples were then mixed to produce samples with identical protein concentrations but containing different amounts of GdnHCl. After 20 min of equilibration, spectra were recorded of both samples, and the procedure was repeated until mixing resulted in solutions of ca. 2.0 M GdnHCl. Far-UV CD spectra were recorded from 250 to 210 nm. Temperature-induced unfolding was followed by monitoring the change in ellipticity at 222 nm of 20 μM solutions of protein in 100 mM NaP_i, pH 7.0. Samples were heated using a scan rate of 45 °C/h. The changes in ellipticity (θ) at 222 nm were analyzed as described previously (*13*).

Equilibrium Denaturation Monitored by Fluorescence. The GdnHCl transition curve at 20 °C was again obtained using the Job method, by mixing samples of protein in 0 and 4 M GdnHCl. For the thermal unfolding experiments the emission spectra were recorded from 5 to 90 °C in steps of 5 °C and in the region of the midpoint in steps of 2.5 °C for the mutants F2W, F22W, and F29W. GdnHCl and heat-induced denaturation was monitored by the change in fluorescence intensity at 344 nm for F2W, 320 nm for F22W, 353 nm for the GdnHCl-induced unfolding of F29W, and 320 nm for the thermal unfolding of F29W. The transition curves were fitted to the two-state model (except that of F22W; see below) as described previously (*13*).

Singular Value Analysis of the Equilibrium Fluorescence GdnHCl Denaturation Curves. The unfolding of F22W by GdnHCl, followed by fluorescence, was analyzed by singular value decomposition (svd) using the routine built into the Matlab software (The Mathworks, Inc., Natick, MA). This analysis yielded three main components (with singular values of 2.7×10^4, 7.6×10^3, and 4.7×10^2), the other components containing only noise (singular values below 1.9×10^1). The GdnHCl dependencies of the three main components were linearly combined and fitted to a three-state model

$$N \overset{K_1}{\rightleftharpoons} I \overset{K_2}{\rightleftharpoons} U$$

to obtain populations of unfolded, native, and intermediate states along with the equilibrium ΔG_0 and *m*-values. The fractions of the different species were taken as

$$\text{native: } \frac{1}{1 + K_1 + K_1K_2}$$

$$\text{intermediate: } \frac{1}{1/K_1 + 1 + K_2}$$

$$\text{unfolded: } \frac{1}{1/(K_1K_2) + 1/K_2 + 1}$$

and the thermodynamic parameters were calculated as

$$K_1 = \exp\left(\frac{m_1[\text{GdnHCl}] - \Delta G_{0,1}}{RT}\right)$$

and

$$K_2 = \exp\left(\frac{m_2[\text{GdnHCl}] - \Delta G_{0,2}}{RT}\right)$$

The corresponding fluorescence spectra were calculated by inversion of the coefficient matrix and by linear combination of the first three spectral components.

Measurements of Unfolding and Refolding Kinetics. Stopped-flow far-UV CD measurements at 222 or 225 nm (far-UV) were performed in Oxford on a BioLogic stopped-flow CD machine equipped with double detection for both CD and fluorescence. HPr (2 mg/mL) in 6.0 M GdnHCl was mixed rapidly to give an 11-fold dilution in 100 mM NaP_i, pH 7.0, buffer to initiate refolding at 20 °C. Under these conditions the ellipticity at 225 nm, as well as the total fluorescence above 314 nm (using an excitation wavelength of 225 nm), was simultaneously detected. Refolding kinetics were fitted to either a single- or double-exponential function.

Stopped-flow fluorescence experiments were carried out in Oxford using a BioLogic SFM3 mixer (Claix, France) with a 2×2 mm cell (BioLogic FC-20) and a BioLogic PMS-400 detection system. Fluorescence anisotropy was detected after excitation at 297 nm (4 nm slit widths) using a newly developed procedure employing a photoelastic modulator on the excitation pathway, a single detector with a WG 335 cutoff filter (Schott Glaswerke, Mainz, Germany), but no polarizer on the emission pathway (*25*). In the experiments involving just fluorescence intensity detection (F22W at different emission wavelengths) an excitation wavelength of 280 nm (4 nm slit widths) was used, and the emission spectrum was recorded using different cutoff filters (WG 305, WG 320, WG 335, WG 360). For fluorescence quenching experiments, the proteins were dissolved at 1 mg/mL in 5 M GdnHCl and mixed with 8.15 volumes of refolding buffer. Different quantities of NaI and NaCl between 0 and 300 mM were added to the refolding buffer so that the ionic strength was maintained at a constant value.

For refolding experiments, the proteins were initially dissolved at 2.5 mg/mL in 6 M GdnHCl and then mixed with 10 volumes of refolding buffer (100 mM phosphate buffer, pH 7.0). Some experiments were also conducted by mixing the proteins with 15.6 volumes of buffer to refold in solutions containing 0.36 M instead of 0.54 M GdnHCl. For the unfolding experiments with F22W at different emission wavelengths, the initial protein concentration was 0.5 mg/mL in buffer and was diluted with 4 volumes of 5 M GdnHCl. The traces obtained by monitoring the fluorescence intensity of F22W during unfolding using different cutoff filters were analyzed simultaneously with Origin software by carrying out a global fit for which the rate constants were invariant among the different data sets but with different amplitudes for each spectral condition. The amplitudes generated by the fitting procedure were then used to calculate the fluorescence emission spectrum for the burst-phase intermediate along the unfolding pathway.

Simultaneous analysis of the kinetic traces of the fluorescence intensity and of the fluorescence anisotropy was carried out using the Origin software using a theoretical approach described previously (*26*). The two kinetic traces were fitted to a reaction scheme involving two states, in the case of F48W, or three states for the three other mutants. The states were characterized by their fluorescence quantum yield (q_i) and their anisotropy level (r_i). The observed fluorescence intensity was calculated as $S(t) = \sum_i x_i(t)q_i$, where $x_i(t)$ is the fraction of species in state *i* at time *t*. The observed fluorescence anisotropy was calculated as $r(t) = (\sum_i x_i(t)r_iq_i)/(\sum_i x_i(t)q_i)$. The fitting procedure provides values for the rate constant of the process being monitored, for the quantum yields (q_i), and for the anisotropy levels (r_i). It is noteworthy that the time dependence of the anisotropy is nonexponential as it results from a ratio of two terms, each having exponential behavior (*25*, *26*).

Mapping the ANS Binding Site. Two-dimensional (2D) $^1H-^{15}N$ heteronuclear single-quantum correlation (HSQC) spectra at 600 MHz were recorded in Groningen of samples containing 1.1 mM ^{15}N-enriched HPr in 100 mM sodium phosphate, pH 7.0 (H_2O/D_2O: 93%/7%), at 20 °C on a Varian Inova 600 spectrometer. Small aliquots of a 25 mM ANS stock solution were gradually added before the spectra were recorded. ^1H chemical shifts are quoted relative to DSS, and ^{15}N chemical shifts are expressed relative to liquid ammonia (*27*). Time-proportional phase incrementation (TPPI; *28*) was used to discriminate between positive and negative ω_1 (^{15}N) frequencies. Typically, in the HSQC experiments the maximum t_1 and t_2 values were 128 and 154 ms, respectively, and the spectral widths in the ω_1 (^{15}N) and ω_2 (^1H) domains were 2000 and 8000 Hz. The ^1H carrier frequency was positioned on the water resonance, and during the acquisition period ^{15}N decoupling was achieved by a broad-band Waltz decoupling sequence. The water resonance

Table 1: K_m Values of the Phosphotransferase Reaction from HPr to Enzyme IIA^{Mtl}, Molar Extinction Coefficients, Average Lifetimes, and Correlation Times of the Major Rotameric State for the WT and Single-Tryptophan Mutants of HPr[a]

protein	K_m (μM)	ϵ_{280} (M^{-1} cm^{-1})	average lifetimes (ns)	correlation times (ns)
WT	6.0 ± 0.6	*b*		
F2W	5.6 ± 0.6	5823	3.3 (3.4)	4.5 (5.3)
F22W	7.2 ± 0.7	6055	2.3 (2.4)	3.7 (4.0)
F29W	8.5 ±1.3	5750	0.46 (0.53)	
F48W	18.0 ± 1.6	5276	2.3 (2.2)	2.4 (2.2)

[a] Details are described in the text. Values in parentheses correspond to those of the phosphorylated forms. [b] In the absence of tryptophan residues, $\epsilon_{259} = 1900$ was used to calculate the protein concentration.

was suppressed using gradients. SNARF (Frans van Hoesel) was used to process, visualize, and analyze these NMR data sets.

RESULTS

Characterization of the HPr Mutants. (i) Phosphoryl-Transfer Function Measurements and Determination of Molar Extinction Coefficients. Table 1 summarizes a range of parameters that characterize the different HPr mutants. The K_m value of 6.0 ± 0.6 μM for the phosphoryl-transfer function of the WT protein is in excellent agreement with the value of 6.3 μM reported previously (*29*). The K_m values of F2W, F22W, and F29W (5.6−8.5 μM) are similar to the value for WT HPr. Thus, the phosphoryl-transfer function of these mutants is comparable to the phosphoryl-transfer function of WT HPr. F48W, however, shows a 3-fold increase in phosphoryl-transfer function compared to WT HPr, indicating that the interaction with the A-domain of enzyme II of the mannitol transport (IIA^{Mtl}) is perturbed by the replacement of the phenylalanine for a tryptophan residue at this position. Residue 48 is known to be at the binding interface of HPr with EII^{Mtl} (*30*); the change in side-chain character is therefore likely to account for the observed change in the phosphoryl-transfer function.

(ii) Steady-State Fluorescence Spectroscopy. The fluorescence characteristics of a tryptophan residue are highly dependent on its microenvironment (*31*). The fluorescence emission maximum varies from 320 nm in an apolar solvent to 350 nm in water. The emission maximum of a single-tryptophan-containing protein therefore enables the polarity in the vicinity of the tryptophan residue to be assessed. Figure 2 shows the emission spectra of the four single-tryptophan mutants of HPr. The emission spectrum of F48W is the most red shifted, showing an emission maximum at 355 nm, corresponding to the value of a free tryptophan residue in water. This result indicates that this tryptophan residue is highly exposed in the protein, in good agreement with the structure of WT HPr where the side chain of Phe48 projects into the solvent (see Figure 1). The emission spectrum of F22W is the most blue shifted with an emission maximum of 326 nm, indicating that the tryptophan residue at this position is in a highly hydrophobic environment, again in good agreement with the structure of WT HPr where the ring of Phe22 is incorporated fully into the hydrophobic core.

F29W has an emission maximum at 342 nm. The aromatic ring of Phe29 in WT HPr is partly buried in the hydrophobic core, consistent with the red shift of the emission maximum of this mutant with respect to the emission maximum of F22W. The tryptophan fluorescence is also highly quenched, most probably by His76 that is in close proximity in the structure (Figure 1). The emission spectrum of F2W shows a maximum at 346 nm. Phe2 is situated at the beginning of the first β-strand in the native HPr structure and is only partially buried, explaining the fact that the emission maximum is closer to the value characteristic of a free tryptophan residue in water.

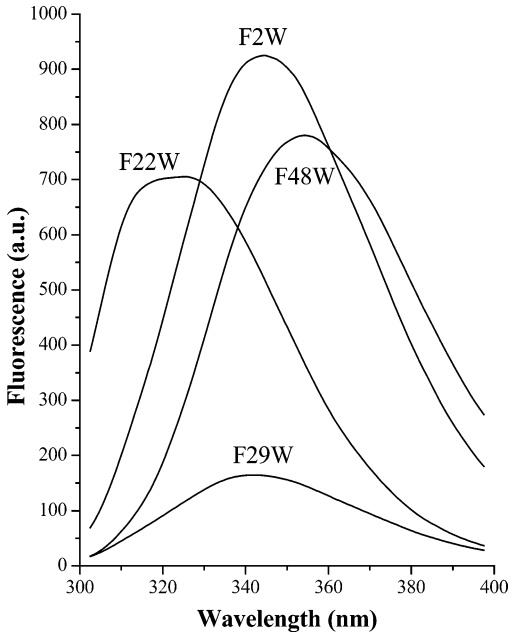

FIGURE 2: Fluorescence emission spectra of the four single-tryptophan HPr mutants at 20 °C. The concentration of the mutant proteins was ca. 3 μM in 100 mM NaP_i buffer, pH 7.0.

The mutant HPr proteins were phosphorylated by phosphoenolpyruvate (PEP) and catalytic amounts of enzyme I (EI). These spectra of the resulting derivatives are essentially identical to the spectra of the nonphosphorylated forms (data not shown), leading to the conclusion that no significant structural changes take place at the mutated sites upon phosphorylation.

(iii) Time-Resolved Fluorescence Spectroscopy. Time-resolved fluorescence spectroscopy specifically monitors the mobility and structural flexibility of proteins. As a consequence of the existence of different rotameric states of the indole moiety, a tryptophan residue can possess multiple fluorescence lifetimes. Each state is represented by a discrete excited-state lifetime (*32*), and in a protein the distribution over these states and the value of the lifetime depend on the protein structure and the microenvironment in which the tryptophan residue is located. Analysis of the fluorescence intensity decay results in a distribution of fluorescence lifetimes; the analysis of the fluorescence anisotropy decay produces a distribution of correlation times associated with different tryptophan rotational modes (*19*). The results of the various measurements obtained in the present study are collected in Table 1.

The correlation times of F2W and F22W, 4.5 ± 0.2 and 3.7 ± 0.3 ns, respectively, correspond closely to the expected rotational correlation time for a protein of the size of HPr (a hydrodynamic radius of 17 Å corresponds to a correlation

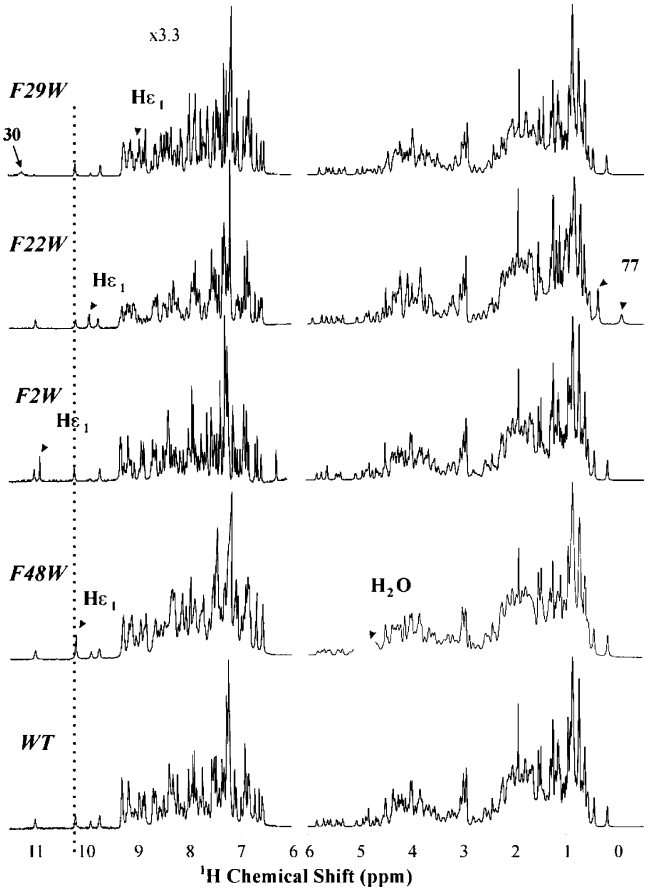

FIGURE 3: 1D ^{1}H NMR spectra of the four single-tryptophan mutants of HPr in comparison to the spectrum of the WT protein. The spectrum of F48W was recorded at 600 MHz in H_2O, while all other spectra were recorded at 750 MHz in H_2O and in D_2O. The downfield regions (11.3−6.0 ppm) are from the 750 MHz spectra recorded in H_2O; the upfield regions (−0.5−6.0 ppm) are from the 750 MHz spectra recorded in D_2O. For clarity, the downfield region of each spectrum is scaled in the vertical axis by a factor of 3.3 relative to the corresponding upfield region. The dotted line represents the position of the random coil chemical shift of the tryptophan indole proton (*44*).

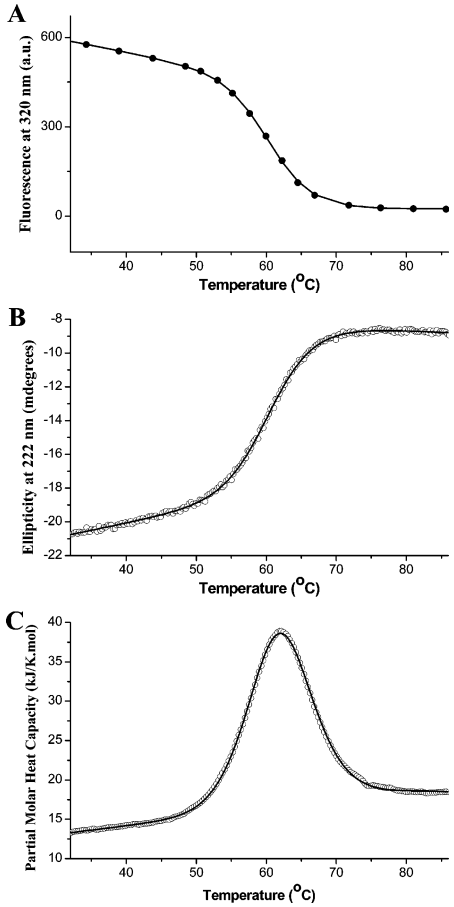

FIGURE 4: Thermal-induced denaturation of F22W monitored by different techniques: (A) intrinsic fluorescence, (B) far-UV CD, and (C) DSC. The solid lines represent the fits of the data to a two-state folding model.

time of 4.4 ns at 20 °C using Stokes' law; *33*) showing that these residues are rigidly held within the protein structure. The immobility of the Trp22 side chain within the protein is most likely to result from the restriction of the side-chain motion as a consequence of the large number of contacts within the hydrophobic core of the protein. Trp2 is, however, only partially buried, and in this case the rigidity might be due to the formation of a hydrogen bond between the indole proton of the tryptophan residue and a carbonyl group of the protein backbone. The observed downfield shift in the NMR spectrum from the random coil chemical shift of this proton in F2W (see Figure 3) is consistent with its involvement in a hydrogen bond. The very short average lifetime of F29W ($\langle\tau\rangle$ is 0.46 ns, a value 5−6 times shorter than for the other mutants; Table 1), as a result of the internal quenching agent discussed above, means that the anisotropy analysis for this mutant is unreliable. F48W, however, has a correlation time of 2.4 ± 0.2 ns and is therefore less restricted in its side-chain motion than F2W and F22W, a result that is entirely consistent with the significant solvent exposure of the side chain of Phe48 in the WT structure (see Figure 1).

Phosphorylation of the mutant proteins has no significant effect on the fluorescence lifetimes and correlation times of the various tryptophan residues (Table 1), a finding in agreement with the results of the steady-state fluorescence measurements and the observation that the only structural changes upon phosphorylation of the WT HPr take place in the vicinity of the active site (*34*).

(iv) Nuclear Magnetic Resonance (NMR) Spectroscopy. Figure 3 shows 1D ^{1}H NMR spectra of the various mutants along with the spectrum of WT HPr. The spectra show a high degree of similarity to each other, indicating that no gross structural changes have taken place upon mutation, although small changes in chemical shifts are observed for protons in the proximity of the mutation sites. For example, in the spectrum of F29W, the amide proton of Thr30 at ca. 11 ppm is shifted downfield by 0.2 ppm, and the resonance is broadened. In the spectrum of F22W, the methyl group resonance of Leu77 at ca. 0.2 ppm is shifted upfield by 0.3 ppm, and the line is again broadened. The resonance broadening in these two cases could be a result of the slow interconversion of different rotameric states of the tryptophan residue at these positions. The large deviations from random coil chemical shifts observed for these resonances are due to the close proximity of the protons to the aromatic rings of the phenylalanine residues at positions 22 and 29, respectively, in the WT HPr structure (*10*) and make them particularly sensitive to conformational changes. In addition, the four mutants show photochemically induced dynamic

Table 2: Thermodynamic Parameters Obtained from Two-State Fits of the Thermally Induced and GdnHCl-Induced Denaturation of WT HPr and the Four Mutants Monitored by DSC, Far-UV CD, and Fluorescence

	F2W[a]	F22W[b]	F29W[a]	F48W[c]	WT[d]
$\Delta G(H_2O)$ (kJ mol^{-1})	21.5 ± 3.0		16.1 ± 0.1	20.3 ± 0.4	20.8 ± 1.5
m-value (kJ mol^{-1} M^{-1})	11.4 ± 1.5		9.5 ± 0.1	9.7 ± 0.2	10.0 ± 1.0
C_m (M)	1.88 ± 0.01		1.69 ± 0.01	2.09 ± 0.06	2.09 ± 0.07
ΔH_m (kJ mol^{-1})	310 ± 5	295 ± 3	269 ± 20	332 ± 1	323 ± 3
T_m (°C)	64.2 ± 0.8	61.4 ± 1.0	59.8 ± 0.7	65.2 ± 1.1	64.6 ± 0.1

[a] Mean values and standard deviations of $\Delta G(H_2O)$, *m*-value, and C_m from far-UV CD and fluorescence data. Mean values and standard deviations of ΔH_m and T_m from DSC, far-UV CD, and fluorescence data. [b] For $\Delta G(H_2O)$, *m*-value, and C_m, see Table 3. Mean values and standard deviations of ΔH_m and T_m from DSC, far-UV CD, and fluorescence data. [c] $\Delta G(H_2O)$, *m*-value, and C_m from far-UV CD only (fitting error given). Mean values and standard deviations of ΔH_m and T_m from DSC and far-UV CD data. [d] Mean values and standard deviations of $\Delta G(H_2O)$, *m*-value, C_m, ΔH_m, and T_m from Table 1 in ref *13*.

nuclear polarization (photo-CIDNP) effects that are consistent with the positions of the corresponding tryptophan residues in the protein structure (*35*).

Folding and Unfolding under Equilibrium Conditions. (i) Heat-Induced Denaturation. Figure 4 shows the transition curves for the thermally induced denaturation of F22W monitored by fluorescence, far-UV CD, and DSC. The thermodynamic parameters that result from fitting the curves shown in Figure 4 to a two-state folding model, and similar data for the other mutant proteins, are given in Table 2. The thermodynamic parameters ΔH and T_m of F48W are closely similar to those of the WT protein and are typical of a globular protein of the size of HPr (*36*, *37*). The transition curve of F2W is shifted slightly toward lower temperature relative to the WT protein. The transition curves for F22W (Figure 4) and F29W, however, show a significant shift toward lower temperature. The transition midpoints T_m for the latter two mutants are 61.4 and 59.8 °C, respectively, in comparison to 64.6 °C for the WT protein and 65.2 °C for F48W. The phenylalanine residues at positions 22 and 29 are situated in the hydrophobic core, and the introduction of the more bulky tryptophan residues probably results in a degree of disruption of the core and thereby lowers the conformational stability of these mutant proteins.

(ii) GdnHCl-Induced Denaturation. Figure 5 shows the fluorescence emission spectra recorded during the GdnHCl-induced unfolding of F22W and F29W. Generally, when a protein unfolds, tryptophan residues become increasingly water accessible, and the intensity of the fluorescence emission is decreased due to a higher rate of internal conversion (*38*). In addition, the emission maximum is shifted to a higher wavelength, because the microenvironment of the tryptophan residue becomes more polar. This is the case for F22W, but F29W shows very different behavior: the emission maximum is indeed shifted to the value of a free tryptophan residue in water, but the intensity of the fluorescence emission is increased in respect to its intensity in the native state. We interpret this latter effect as resulting from the loss of the internal quenching of His76 when unfolding of the protein takes place.

For all four mutants studied here the GdnHCl-induced unfolding transitions were found to be fully reversible. The GdnHCl-induced denaturation transitions of all mutants, except those of F22W, monitored by fluorescence and CD, were fitted to a two-state model, and the parameters resulting from the fits are listed in Table 2. The thermodynamic parameters derived from the fluorescence data are in good agreement with the values of these parameters derived from

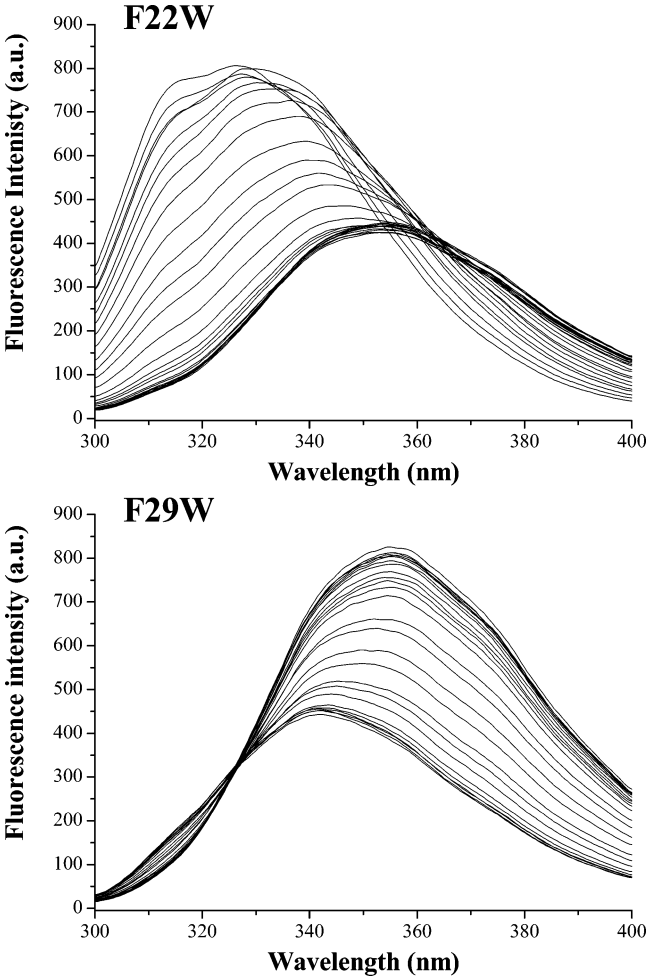

FIGURE 5: GdnHCl denaturation followed by fluorescence for the F22W and F29W mutants of HPr. Emission spectra were recorded of samples containing various concentrations (between 0 and 4.0 M) of GdnHCl (see text).

CD. F48W and WT HPr show similar unfolding behavior, as expected from the position of residue 48 at the surface of the native protein with its side chain projecting into the solvent (see Figure 1). The transition curves for these proteins coincide closely, and the transition midpoints and energies are the same within the error of the experiments. The transition curves of F2W are, however, slightly shifted toward lower GdnHCl concentrations, resulting in a C_m of 1.88 ± 0.01 M rather than 2.09 ± 0.07 M for the WT and F48W. The value of $\Delta G(H_2O)$, however, is 21.5 ± 3 kJ mol^{-1} and is somewhat higher than the value of the WT protein (20.8 ± 1.5 kJ mol^{-1}). The typical β-strand NOE patterns found

Table 3: Thermodynamic Parameters Resulting from a Three-State Fit of the Equilibrium Unfolding Transition of F22W in Increasing Concentrations of GdnHCl Measured by Fluorescence

	m-value (kJ mol^{-1} M^{-1})	ΔG_0 (kJ mol^{-1})	C_m (M)
N ↔ I	4.8 ± 0.3	3.7 ± 0.2	0.77 ± 0.05
I ↔ U	8.3 ± 0.2	13.2 ± 0.5	1.59 ± 0.06

for residue 2 in the NOESY spectra of F2W are unchanged (data not shown), indicating that the β-sheet structure in this region is intact following the mutation. The higher conformational stability of F2W could be a result of a stabilization of the interaction between the first β-strand and the C-terminal helix. The values of $\Delta G(H_2O)$ for F29W and for F22W, as will be discussed below, are substantially lower than for WT HPr, in agreement with the lower ΔH and T_m values obtained from the thermally induced unfolding transitions.

Some of the thermodynamic parameters listed in Table 2 show large standard deviations that are the result of discrepancies between the parameters derived from CD and from fluorescence. These discrepancies could be due to the differences in the properties of the protein that are monitored by the different techniques. Far-UV CD detects the change in secondary structure (here mainly α-helical structure), while fluorescence monitors the change in local structure around the fluorescence probe. It has been demonstrated previously that considerable care should be taken in extracting thermodynamic parameters from fluorescence data due to the intrinsic complexity of the factors that influence the measurements (*31*, *38*).

In contrast to the situation with the other three mutants, the fluorescence changes associated with the equilibrium unfolding of F22W by GdnHCl do not show the isofluoric point expected for a two-state transition (see Figure 5A). Rather, the early spectra reveal a shift in the emission maximum prior to the major unfolding transition that takes place at higher GdnHCl concentrations. We therefore used a singular value decomposition method to analyze these data (*39*). This procedure yielded three principal components, which were subsequently linearly combined to fit a three-state equilibrium model. The fit gives values for the free energies and *m*-values of the two transitions (Table 3) and allows the spectra and GdnHCl transition curves of the native, unfolded, and intermediate states to be calculated. These transition curves are shown in Figure 6A and the corresponding fluorescence spectra in Figure 6B. The sum of the $\Delta G(H_2O)$ values of the two processes (16.9 ± 0.5 kJ mol^{-1}) is the same, within experimental error, as the value obtained from the CD data (17.6 ± 0.8 kJ mol^{-1}) that were fitted to a two-state model. It is important to note, however, that in the absence of GdnHCl at 20 °C F22W is not fully in its native state, as can be seen from the relative populations of native and intermediate species at the first data point in Figure 6A.

The analytical procedure we have used here allows us, however, to calculate the spectrum of the native state by extrapolation to a hypothetical condition where the latter is fully populated. This spectrum is shown in Figure 6B where the experimental fluorescence scans obtained for the proteins in 0 and 4 M GdnHCl are plotted as broken lines next to the calculated spectra. The experimental data obtained in the

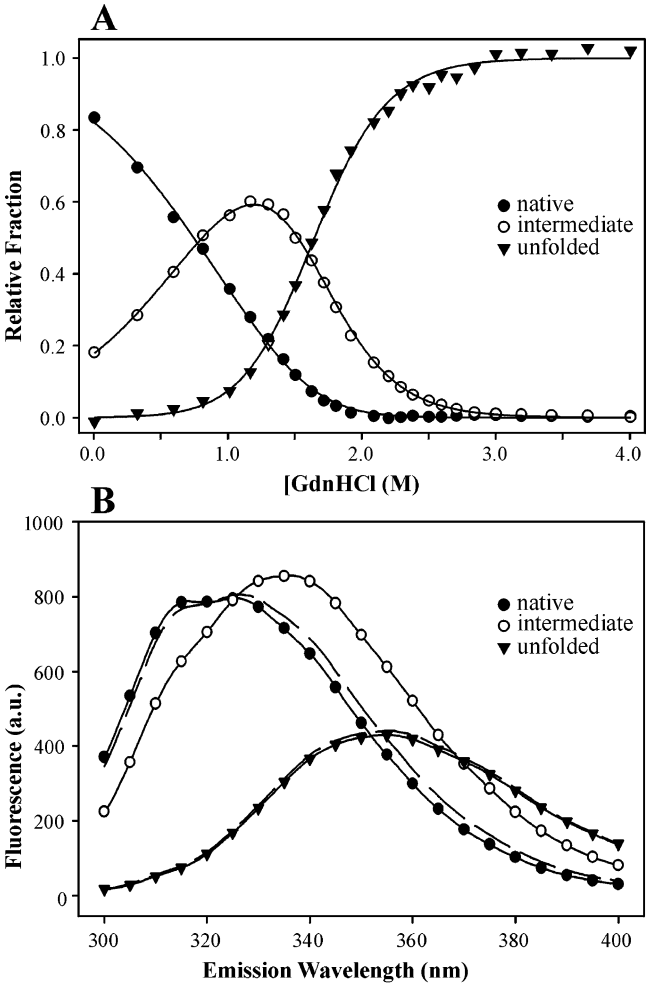

FIGURE 6: Singular value decomposition of the equilibrium unfolding of the F22W mutant by GdnHCl followed by fluorescence shown in Figure 5. (A) Data points after singular value decomposition (see text) for the native (●), intermediate (○), and unfolded (▼) states. The corresponding fits generated by an equilibrium three-state model are displayed as solid lines. (B) Reconstructed fluorescence spectra after singular value decomposition (see text) for the native (●), intermediate (○), and unfolded (▼) states. The experimental spectra of F22W in the absence of GdnHCl and in the presence of 4 M GdnHCl are displayed as broken lines.

absence of GdnHCl are slightly shifted toward the intermediate state spectrum as compared with the calculated native state spectrum, as a result of the populations shown in Figure 6A. By contrast, the unfolded spectrum and the data obtained in 4 M GdnHCl are much closer to each other, the small differences probably reflecting the effect of GdnHCl on the fluorescence spectrum in absence of a conformational change, as our analysis did not include pre- or posttransition baseline slopes (*25*, *40*). The native state spectrum and, to a lesser extent, the intermediate state spectrum show an additional peak centered around 314 nm; this is probably the Raman peak from solvent water under the excitation conditions used here (280 nm with 5 nm slit width).

In Figure 6B, the spectrum of the intermediate state is somewhat red shifted compared to the native state, with a slight increase in the fluorescence quantum yield. This observation is likely to reflect the fact that Trp22 is more exposed to water in the intermediate state than in the native state, as a blue shift in tryptophan emission in native proteins is normally attributed to shielding of the residue from water

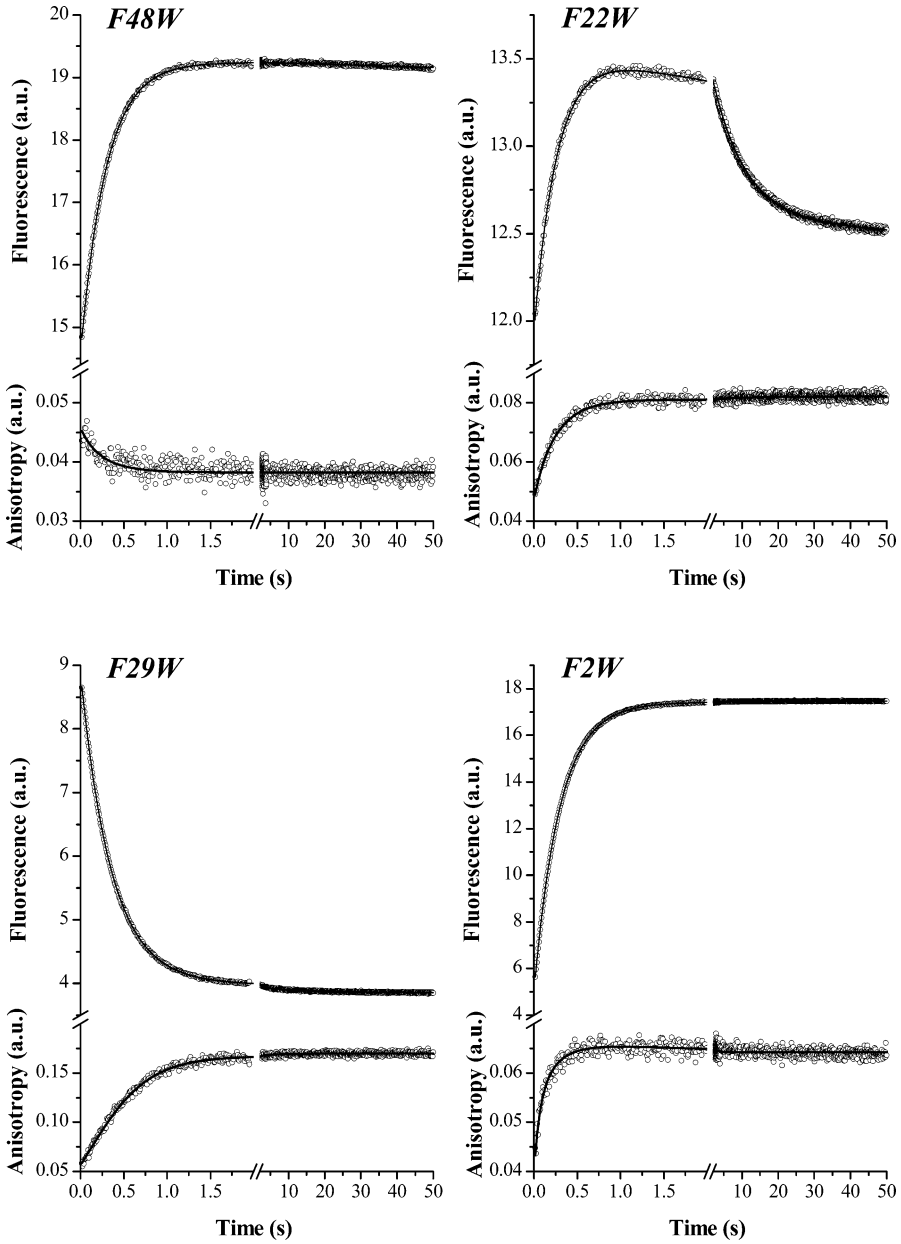

FIGURE 7: Stopped-flow fluorescence intensity and anisotropy traces characterizing the refolding of the four single-tryptophan mutants of HPr in 0.54 M GdnHCl at 20 °C and pH 7.0. The fits resulting from the global analysis (see Materials and Methods) are displayed.

(*31*). The change in quantum yield must reflect the difference in quenching processes that Trp22 experiences in the different states (*31*). Thus, we can conclude that the initial step in the unfolding of F22W by GdnHCl involves an opening of the structure in this region of the protein, thereby increasing the accessibility of the Trp22 side chain to the solvent. This result is in very good agreement with equilibrium studies on the WT HPr (*13*) that show that the hydrophobic dye ANS has an initial increase in fluorescence on binding to the protein in GdnHCl concentrations of up to 1.2 M; the latter is exactly the concentration at which the intermediate state detected in the present study is at its maximum population (Figure 6A).

Kinetic Folding and Unfolding Measurements. (i) Refolding of the Mutants Followed by Measurements of Stopped-Flow Fluorescence Anisotropy. The refolding of the HPr mutants was studied at pH 7.0, 20 °C, and 0.54 and 0.36 M GdnHCl by stopped-flow fluorescence by measuring the total fluorescence intensity and its anisotropy. The intensity changes obtained during refolding in 0.54 M GdnHCl are shown in Figure 7; the parameters resulting from the kinetic analysis are given in Table 4.

The initial and final fluorescence intensities are in good agreement with equilibrium measurements presented above, the F29W showing a fluorescence decay that can be associated with the presence of His76, which acts as an internal quenching agent as it is located in close proximity to this residue in the native state. All of the fluorescence traces show a fast phase that coincides with the single phase observed in the far-UV CD stopped-flow measurements. The rate constant of this phase ranges from 2.86 to 3.80 s^{-1} in the various mutants and corresponds well to the rate measured for the WT protein by far-UV CD under the same conditions (3.3 ± 0.3 s^{-1}). The refolding of F29W, F2W, and F22W shows an additional slow phase, most evident for F22W. For F29W, and even more so for F2W, the amplitude of the slow phase is not large enough (it is less than 3% of that of the first phase) to allow an accurate measurement of the corresponding rate constant. This slow

Table 4: Kinetic Parameters Resulting from the Analysis of the Stopped-Flow Fluorescence Intensity and Fluorescence Anisotropy Experiments for the Four Single-Tryptophan Mutants of HPr in 0.54 and 0.36 M GdnHCl at pH 7.0 and 20 °C[a]

		A_1(% U−N) fluorescence	A_1(% U−N) anisotropy	k_1 (s^{-1})	A_2(% U−N) fluorescence	A_2(% U−N) anisotropy	k_2 (s^{-1})
0.54 M GdnHCl	F2W	99.1	108.9	3.42	0.9	−8.9	0.73
	F22W	246	96.5	3.80	−146	3.5	0.11
	F29W	−97.1	96.7	2.86	−2.9	3.3	0.23
	F48W	100	−100	3.42			
0.36 M GdnHCl	F22W	346.7	94.2	7.31	−446.7	5.8	0.12
	F29W	−96.6	96.7	5.24	−3.4	3.3	0.44
	F48W	100	−100	6.43			

[a] A_1 and k_1 are the amplitude and rate constant, respectively, of the major refolding phase; A_2 and k_2 are those of the second slower phase. Negative amplitudes reflect a signal decrease. The error in the rate constants is estimated to be in the order of 5%.

phase has been seen in the study of the refolding of the WT protein only when monitored by the hydrophobic dye ANS where a rate constant of 0.09 ± 0.01 s^{-1} was measured (*13*), a value very close to the rate measured here for F22W (0.11 ± 0.01 s^{-1}), the mutant protein whose fluorescence behavior shows the most significant amplitude for this slow phase. We interpret this slow phase as a slow rearrangement of the rigidly formed initial structural core of the protein, in which residue 22 is located, that probably involves exclusion of solvent molecules and also of the ANS dye when present. This conclusion is in good agreement with equilibrium measurements that show that the unfolding of F22W monitored by fluorescence is not cooperative and that a red-shifted intermediate is detected in this protein at GdnHCl concentrations early before the unfolded state is significantly populated (see above).

Finally, it can be seen from Table 4 that the effect of GdnHCl concentration on the rate of the slow refolding phase of F22W is negligible (it changes from 0.11 to 0.12 s^{-1} when the final GdnHCl concentration is changed from 0.54 to 0.36 M), whereas it almost doubles the rate of the major refolding step (from 3.8 to 7.3 s^{-1} when the final GdnHCl concentration is changed from 0.54 to 0.36 M). This finding is again in good agreement with the dependency of the refolding rates on GdnHCl concentration observed for the WT protein refolded in the presence of ANS (*13*). This result further supports the assumption that the slow phase involves a local rearrangement of tertiary structure and as such is not very sensitive to changes in the denaturant concentration.

The kinetic traces in the fluorescence anisotropy refolding experiments with the mutants are also shown in Figure 7. As for the fluorescence intensity traces, the native anisotropy values are in good agreement with steady-state measurements: the time-resolved fluorescence measurements discussed above show that the correlation times of F2W and F22W, and therefore their native state anisotropy values measured here, correspond to the rotation of a protein of the size of HPr. Internal quenching of the fluorescence of F29W means that the lifetime of this residue is very short, and therefore the anisotropy value is anomalously high. Finally, the anisotropy value of the native state of F48W is very low, in agreement with the time-resolved fluorescence measurements, reflecting the location of this residue at the surface of the protein, projecting into the solvent.

The global analysis procedure we have used for the stopped-flow fluorescence data (see Materials and Methods) allows us to extract specific values for the anisotropy changes occurring during the fast and slow phase of folding (Table 4). Even in the case of F22W, for which the changes in fluorescence intensity are of the same order of magnitude in the two phases, the change in anisotropy during the slow phase is much smaller than the change observed during the fast phase. This finding is in good agreement with the assumption that the tertiary structure in the folding intermediate is very nativelike and that the mobility of the probe is almost as restricted in the intermediate as it is in the native state. The fluorescence intensity changes involve principally in a shift of the emission spectrum, as observed under equilibrium conditions. As we shall show below by the use of multiple cutoff filters in the experiments, the changes are due to modifications of the polarity around the probe induced by solvent exclusion from the protein core.

(ii) Kinetic Unfolding Monitored by Stopped-Flow Fluorescence. The unfolding kinetics of F22W, F29W, and F48W were studied by stopped-flow fluorescence measurements at 20 °C, 4 M GuHCl, and pH 7.0 (data not shown). The fluorescence intensity changes are all satisfactorily described by single-exponential functions, with time constants of 185, 63, and 800 ms for F22W, F29W, and F48W, respectively. Under conditions similar to those used here, the WT protein has a time constant of 1000 ms (*13*). From Table 4, it can be seen that all four mutants refold with a time constant for the main phase between 0.26 and 0.35 s in 0.54 M GdnHCl, compared with 0.30 s for WT HPr under similar conditions. Therefore, the folding process, in contrast to the unfolding reaction, is only marginally affected by the mutations. From the equilibrium stability measurements it can be seen, however, that the mutants F29W and F22W are significantly destabilized respective to the WT protein (4.7 and 3.9 kJ mol^{-1}, respectively; Tables 2 and 3), whereas F2W and F48W have stabilities closer to that of the WT protein. The unfolding results presented here show that the destabilization of F29W and F22W occurs mainly through an increase in the unfolding rate. F48W serves as a control for which neither the folding nor the unfolding rate is modified significantly relative to the WT protein.

(iii) Unfolding of F22W Studied at Different Emission Wavelengths. To relate the kinetics of unfolding of F22W obtained from the stopped-flow measurements to the equilibrium unfolding properties of this mutant in GdnHCl, we studied its unfolding by measurement of stopped-flow fluorescence intensity using different wavelength filters. In all cases the unfolding traces show an initial overshoot in the dead time of the stopped-flow experiment (data not shown), in agreement with the overshoot observed for ANS fluorescence during unfolding experiments with the WT

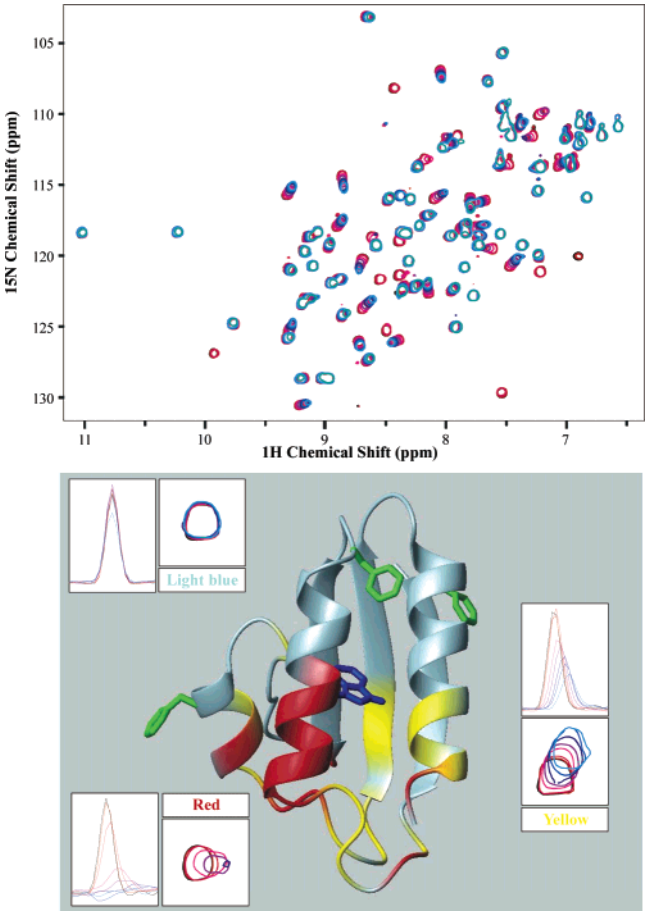

FIGURE 8: NMR determination of the ANS binding site of HPr. Spectral changes in the HPr spectrum as the concentration of ANS is increased were classified into three groups as shown in the inserts and are color coded in the structure as light blue (no/minor changes), yellow (intermediate changes), and red (big changes). For clarity, the side chains of the three phenylalanine residues at positions 2, 29, and 48 and the tryptophan at position 22 are illustrated.

protein (*13*). This approach enables spectral information to be obtained by integrating the fluorescence intensities above a variable set point. By using the transmission curves of the filters and calculating differences between amplitudes obtained using two successive filters, one is able to reconstruct spectral information calculated for the burst-phase intermediate populated during the stopped-flow unfolding experiment. This spectrum (data not shown) is closely similar to that of the intermediate state spectrum under equilibrium conditions deduced from the three-state fit described above (see Figure 6B) and provides an explanation for the overshoot observed in both the present unfolding fluorescence experiments and the ANS experiments on the WT protein.

(iv) Fluorescence Quenching of the F22W Folding Intermediate. To examine whether the observed changes in the equilibrium and kinetic fluorescence data for F22W correspond to those observed in the equivalent ANS binding studies on WT HPr, ANS was titrated into a solution of ^{15}N-labeled HPr, and the effects were monitored by recording a series of HSQC spectra. Figure 8 shows the changes in these spectra as increasing amounts of ANS were added to the solution. Major changes (colored red on the WT structure in Figure 8) were observed in the vicinity of the active site and include shifts of the resonances of Phe22; the resonances of Phe2, Phe29, and Phe48 are, however, unaffected. The chemical shift changes reflect the region where ANS binds to HPr and strongly suggest that the fluorescence changes in Trp22 and the ANS binding studies monitor the same local rearrangement process during the folding reaction. Kinetic refolding studies of WT HPr monitored by the enhancement of ANS fluorescence upon binding show an overshoot in the fluorescence intensity after the first major folding phase, after which the enhancement slowly falls to that of the final native state. The nature of this second phase implies that ANS becomes excluded from the protein structure during this slow process.

We have performed stopped-flow fluorescence refolding experiments on F22W in the presence of increasing concentrations of sodium iodide, a fluorescence-quenching agent (data not shown). Using a simple collision model, a linear relationship is predicted between the concentration of the quenching agent, [Q], and the change in fluorescence intensity, $I_0/I = 1 + K_{sv}[Q]$, where I and I_0 are the intensities in the presence and absence of quenching agent, respectively, and K_{sv} is the effective Stern−Volmer quenching constant, which is the ratio of the rate of collision quenching to the unquenched fluorescence decay rate (*40*). A progressive shielding of the intrinsic fluorescence from solvent is observed as the protein evolves from the unfolded state toward its folded state (data not shown). Even though the tryptophan residue in the folding intermediate has acquired extensive protection from solvent ($K_{sv} = 0.5$ M^{-1}), there is still a further sequestering of the probe from solvent when the native state is reached ($K_{sv} = 0.3$ M^{-1}). This result is in very good agreement with the kinetics of ANS exclusion measured during the refolding of the WT protein.

DISCUSSION

In this paper we have described the use of an integrated approach, involving site-directed mutagenesis in combination with a wide variety of biophysical techniques, to construct a detailed picture of the folding behavior of the small globular protein, HPr. The key step in this approach was to replace systematically and in turn each of the four phenylalanine residues in the protein by single-tryptophan residues, as the latter can readily be monitored by spectroscopic means to provide structural probes in different regions of the native fold.

The replacement of phenylalanine residues with tryptophans at the various sites in the molecule did not result in any substantial structural changes, only localized structural rearrangements around the mutated sites. This conclusion comes from the comparison of each mutant with the WT protein as follows: (i) the phosphoryl-transfer function is maintained in each mutant, (ii) the NMR spectra of all the mutants closely resemble the spectrum of the WT protein, and (iii) the emission fluorescence maxima, correlation times, and lifetimes observed in steady-state and time-resolved fluorescence measurements can be rationalized completely in terms of the positions of the phenylalanines in the three-dimensional structure of the WT protein. All of these observations indicate that the structure simply reorganizes slightly to accommodate the bulkier side chain, making the four single-tryptophan mutants excellent models for the detailed study of the folding of HPr.

Although replacement of the solvent-accessible residue at position 48 did not result in destabilization of the protein,

replacement of the two phenylalanines located in the hydrophobic core (those at positions 22 and 29) did result in lower stability, presumably as a result of slightly less efficient side-chain packing of the structure in the presence of the larger tryptophan side chains. The destabilization of these two mutants occurs mainly as a result of an increase in the unfolding rate, the folding rate being hardly affected. This suggests that these residues, both located in the first helix α1 of HPr, are not significantly structured in the transition state for folding. This conclusion is fully in accord with detailed ϕ-value analyses of two structurally homologous proteins, AcP (*7*) and the activation domain of procarboxypeptidase A2 (ADA2h; *41*). Both studies showed that the central section of the β-sheet is the most structured region in the transition state, as revealed by the relatively high ϕ-values of residues located in this part of the protein, and that interactions formed by the two helices, α1 and α2 (corresponding to the first two helices, α1 and α2, in HPr), appear to be less consolidated.

To study the folding of HPr under a variety of conditions, we used a battery of complementary biophysical techniques, each monitoring different aspects of the changes occurring during the folding process. The thermally induced denaturation of WT HPr and of all four tryptophan mutants, probed by DSC, far-UV CD, and fluorescence, fits well to a simple two-state model of the folding process. Nevertheless, not all of the data obtained for denaturation in GdnHCl can be described by such a simple model. Although the far-UV CD changes induced by addition of GdnHCl are in all cases fully consistent with two-state behavior for the folding of HPr, both in the equilibrium and in the kinetic experiments, other probes such as ANS binding and intrinsic fluorescence show deviation from two-state behavior, indicating the significant population of an intermediate state. This intermediate state strongly resembles the native state in terms of both its overall secondary structure (the two states have the same ellipticity at 225 nm) and its tertiary structure (the two states are indistinguishable in the real-time NMR kinetic experiments; *13*), except in the region of residue 22. This residue is located at the N-terminal end of the first α-helix, and in this region the intermediate has a larger hydrophobic area exposed to the solvent, as indicated by the red shift of the fluorescence emission maximum of the F22W mutant compared to the native state, a higher quantum yield, stronger quenching of the fluorescence by NaI, and the greater enhancement in ANS fluorescence. This near nativelike intermediate state appears to be populated in both the folding and unfolding processes.

Chiti et al. found, by measuring the development of activity during the refolding of the homologous protein AcP, that the fully functional state of the protein takes longer to emerge than optical measurements suggest (*42*). It was found that the slow phase in the recovery of the activity arises from the *cis*−*trans* interconversion of proline 71 in a nativelike intermediate of AcP. Interestingly, the active site of this protein (including residue 23 that is positioned at the N-terminus of the first α-helix of AcP) coincides with the region in HPr found to be perturbed in the intermediate state (see Figure 8). It is possible, therefore, that a similar structural change represents the slow step in the complete folding of the two proteins. HPr contains two prolines at positions 11 and 18, the latter located four residues downstream from Phe22 at the N-terminus of helix α1 and in the perturbed region of the intermediate state of HPr. The accumulation of this near-native state is, however, also observed as an overshoot in the dead time of the kinetic unfolding experiment of the F22W mutant by fluorescence (data not shown) and of the WT protein by ANS binding (*13*). Additionally, the spectrum of the dead time intermediate, deduced from the kinetic unfolding experiment of the F22W mutant using different cutoff filters, was found to be closely similar to that of the intermediate state spectrum under equilibrium conditions deduced from the three-state fit. These findings are not anticipated for proline isomerism. It is likely, therefore, that the slow phase in the folding of HPr has a different structural origin, the nature of which is not yet understood.

Both of these studies suggest, therefore, that although small, single-domain proteins characteristically fold by a mechanism that can broadly be described as being a cooperative two-state process (*4*, *5*), in at least some cases it appears that local structural rearrangements may still be required to complete the folding process. Although the difference between the intermediate state populated prior to the reorganization and the native state may be very small, under some circumstances they could be of considerable significance. For AcP, for example, it is evident that activity is not achieved until the final reorganization steps (*42*), and locally misfolded regions could well contribute in some cases to properties of the protein such as sensitivity to proteolytic cleavage or propensity to aggregate. More generally, this study suggests that care must be taken in making the assumption of the complete cooperativity of the folding of even small proteins on the basis of evidence from a limited number of measurements that provide only a global view of the protein structure. The combination of site-directed mutagenesis and the use of a wide variety of biophysical techniques have led in the case of HPr to a description of the folding behavior of this relatively small globular protein in which local deviations from complete cooperativity are evident.

ACKNOWLEDGMENT

We thank Dolf Swaving-Dijkstra and Ton Visser for recording the time-resolved fluorescence spectra in Wageningen.

REFERENCES

1. Radford, S. E., and Dobson, C. M. (1999) *Cell 97*, 291−298.
2. Pain, R. H. (1999) *Mechanisms in Protein Folding*, 2nd ed., Oxford University Press, Oxford.
3. Myers, J. K., and Oas, T. G. (2002) *Annu. Rev. Biochem. 71*, 783−815.
4. Jackson, S. E. (1998) *Folding Des. 3*, R81−R91.
5. Gunasekaran, K., Eyles, S. J., Hagler, A. T., and Gierasch, L. M. (2001) *Curr. Opin. Struct. Biol. 11*, 83−93.
6. Fersht, A. R. (1999) *Structure and Mechanism in Protein Science*, Freeman, New York.
7. Chiti, F., Taddei, N., White, P. M., Bucciantini, M., Magherini, F., Stefani, M., and Dobson, C. M. (1999) *Nat. Struct. Biol. 11*, 1005−1009.
8. Plaxco, K. W., Simons, K. T., and Baker, D. (1998) *J. Mol. Biol. 277*, 985−994.
9. Postma, P. W., Lengeler, J. W., and Jacobson, G. R. (1993) *Microbiol. Rev. 57*, 543−594.
10. Van Nuland, N. A. J., Hangyi, I. W., Van Schaik, R. C., Berendsen, H. J. C., Van Gunsteren, W. F., Scheek, R. M., and Robillard, G. T. (1994) *J. Mol. Biol. 237*, 544−559.

11. Jia, Z., Quail, J. W., Waygood, E. B., and Delbaere, L. T. J. (1993) *J. Biol. Chem. 268*, 22490−22501.
12. Swindells, M. B., Orengo, C. A., Jones, D. T., Pearl, L. H., and Thornton, J. M. (1993) *Nature 362*, 299.
13. Van Nuland, N. A. J., Meijberg, W., Warner, J., Forge, V., Scheek R. M., Robillard, G. T., and Dobson, C. M. (1998) *Biochemistry 37*, 622−637.
14. Landt, O., Grunert, H. P., and Hahn, U. (1990) *Gene 96*, 125−128.
15. Van Nuland, N. A. J., Van Dijk, A. A., Dijksrtra, K., Van Hoesel, F. H. J., Scheek R. M., and Robillard, G. T. (1992) *Eur. J. Biochem. 203*, 483−491.
16. Robillard, G. T., and Blaauw, M. (1987) *Biochemistry 26*, 5796−5803.
17. Gill, S. C., and Von Hippel, P. H. (1989) *Anal. Biochem. 182*, 319−326.
18. Pace, C. N. (1986) *Methods Enzymol. 131*, 266−280.
19. Visser, A. J. W. G., Van Engelen, J., Visser, N. V., Van Hoek, A., Hilhorst, R., and Freedman, R. B. (1994) *Biochim. Biophys. Acta 1204*, 225−234.
20. Hwang, T.-L, and Shaka, A. J. (1995) *J. Magn. Reson. A112*, 275−279.
21. Privalov, P. L., and Plotnikov, S. A. (1989) *Thermochim. Acta 139*, 257−277.
22. López-Mayorga, O., and Freire, E. (1987) *Biophys. Chem. 27*, 87−96.
23. Privalov, P. L., and Potekhin, S. V. (1986) *Methods Enzymol*. *114*, 4−51.
24. Vigera, A. R., Martinez, J. C., Filimonov, V. V., Mateo, P. L., and Serrano, L. (1994) *Biochemistry 33*, 2142−2150.
25. Canet, D., Doering, K., Dobson, C. M., and Dupont, Y. (2001) *Biophys. J. 80*, 1996−2003.
26. Otto, M. R., Lillo, M. P., and Beechem, J. M. (1994) *Biophys. J. 67*, 2511−2521.
27. Live, D. H., Davis, D. G., Agosta, W. C., and Cowburn, D. (1984) *J. Am. Chem. Soc. 106*, 1939−1941.
28. Redfield, A. G., and Kunz, S. D. (1975) *J. Magn. Reson. 19*, 250−254.
29. Lolkema, J. S., Ten Hoeve-Duurkens, R. H., and Robillard, G. T. (1993) *J. Biol. Chem. 268*, 17844−17849.
30. Van Nuland, N. A. J., Kroon, G. J. A., Dijkstra, K., Wolters, G. K., Scheek, R. M., and Robillard, G. T. (1993) *FEBS Lett. 315*, 11−15.
31. Eftink, M. R. (1991) *Methods Biochem. Anal. 35*, 127−207.
32. Ross, J. B. A., Wyssbrod, H. R., Porter, A. R., Schwartz, G. P., Michaels, C. A., and Laws, W. R. (1992) *Biochemistry 31*, 1585−1594.
33. Lakowicz, J. R. (1983) *Principles of fluorescence spectroscopy*, Plenum Press, New York.
34. Van Nuland, N. A. J., Boelens, R., Scheek, R. M., and Robillard, G. T. (1995) *J. Mol. Biol. 246*, 180−193.
35. Canet, D., Lyon, C., Robillard, G. T., Scheek, R. M., Dobson, C. M., Hore, P. J., and Van Nuland, N. A. J. (2002) (submitted for publication).
36. Privalov, P. L., and Gill, S. J. (1988) *Adv. Protein Chem. 39*, 191−234.
37. Alexander, P., Fahnestock, S., Lee, T., Orban, J., and Bryan, P. (1992) *Biochemistry 31*, 3597−3603.
38. Eftink, M. R. (2000) *Methods Enzymol. 323*, 459−473.
39. Henry, E. R. (1997) *Biophys. J. 72*, 652−673.
40. Itzhaki, L. S., Evans, P. A., Dobson, C. M., and Radford, S. E. (1994) *Biochemistry 33*, 5212−5220.
41. Villegas, V., Martinez, J. C., Aviles, F. X., and Serrano, L. (1998) *J. Mol. Biol. 283*, 1027−1036.
42. Chiti, F., Taddei, N., Giannoni, E., Van Nuland, N. A. J., Ramponi, G., and Dobson, C. M. (1999) *J. Biol. Chem. 274*, 20151−20158.
43. Kraulis, P. J. (1991) *J. Appl. Crystallogr. 24*, 946−950.
44. Bundi, A., and Wüthrich, K. (1979) *Biopolymers 18*, 285−297.

BI027182P